






Metal-rich stars are less suitable for the evolution of life on their planets

Received: 31 August 2022

Accepted: 3 March 2023

Published online: 18 April 2023

 Check for updates

Anna V. Shapiro ¹ ✉, Christoph Brühl², Klaus Klingmüller ², Benedikt Steil², Alexander I. Shapiro ¹, Veronika Witzke¹, Nadiia Kostogryz¹, Laurent Gizon ^{1,3,4}, Sami K. Solanki ^{1,5} & Jos Lelieveld ^{2,6}

Atmospheric ozone and oxygen protect the terrestrial biosphere against harmful ultraviolet (UV) radiation. Here, we model atmospheres of Earth-like planets hosted by stars with near-solar effective temperatures (5300 to 6300 K) and a broad range of metallicities covering known exoplanet host stars. We show that paradoxically, although metal-rich stars emit substantially less ultraviolet radiation than metal-poor stars, the surface of their planets is exposed to more intense ultraviolet radiation. For the stellar types considered, metallicity has a larger impact than stellar temperature. During the evolution of the universe, newly formed stars have progressively become more metal-rich, exposing organisms to increasingly intense ultraviolet radiation. Our findings imply that planets hosted by stars with low metallicity are the best targets to search for complex life on land.

Complex, multicellular life on land requires oxygen (O₂) from which ozone (O₃) forms¹, leading to a tolerable ultraviolet radiation (UV) level at the surface for its development and evolution^{2–4}. Stellar emission and planetary UV protection depend on the effective temperature of the host star^{5–7}. While for a young planet UV exposure can be essential for abiogenesis^{8–11}, high levels of UV trigger genomic damage and are a threat to all life forms^{12–14}. In the Sun-Earth system the UV-C (202 to 230 nm, wavelengths potentially reaching the surface in oxygenated atmospheres) and UV-B (280 to 315 nm) fluxes at 1 Astronomical Unit (au) from the Sun are about 0.76 W/m² and 20 W/m², respectively¹⁵. This is well above the maximum tolerable level for terrestrial life. Land-based life has nevertheless evolved on Earth through oxygen enrichment of the atmosphere that blocks most of the UV radiation. While UV-C is largely absorbed by O₂ molecules in the upper atmosphere, UV-B is absorbed by the ozone layer in the middle atmosphere.

The O₃ concentration is regulated by a photochemical cycle of O₂ and O₃ dissociation by solar UV radiation in the Herzberg continuum (200 to 242 nm) and Hartley band (200 to 320 nm), respectively¹. Only the longer wavelengths (260 to 320 nm) of the Hartley band are relevant for the O₃ column density burden because

radiation at shorter wavelengths is mostly absorbed by O₂. Ozone absorption in the band center (260 nm) is so strong that radiation can hardly penetrate to the middle atmosphere where O₃ concentrations are highest (Supplementary Fig. 1 and 3). Hence, the O₃ concentration depends on the balance between stellar irradiance in the 200 to 242 nm and 260 to 320 nm spectral bands, which govern the production and destruction of O₃, respectively (hereafter we refer to the net photochemical effect). Consequently, the UV-protection provided by the planetary atmosphere depends on the spectral distribution of the stellar radiation^{5,7,16}.

The stellar radiative spectrum, in turn, depends on the effective temperature, T_{eff}, and metallicity, [Fe/H], that represents the abundance of elements heavier than hydrogen and helium in a star (see Eq. 4 in methods section Stellar spectra). The dependence of the radiative conditions at the planetary surface on the stellar effective temperature has been studied previously. For example, it was shown that with increasing effective temperature the planetary surface UV above 290 nm also increases, but the radiative transfer at shorter wavelengths is non-monotonous due to spectrally dependent photochemical effects^{5,7}.

¹Max Planck Institute for Solar System Research, Göttingen, Germany. ²Max Planck Institute for Chemistry, Mainz, Germany. ³Institute for Astrophysics, Georg-August-Universität Göttingen, Göttingen, Germany. ⁴Center for Space Science, NYUAD Institute, New York University Abu Dhabi, Abu Dhabi, UAE. ⁵School of Space Research, Kyung Hee University, Yongin, Republic of Korea. ⁶The Cyprus Institute, Climate and Atmosphere Research Center, Nicosia, Cyprus.

✉ e-mail: shapiro@mps.mpg.de

Here, we investigate the dependence of planetary surface UV on the atmospheric O₂ concentration and stellar metallicity for stars of three spectral types: G2V ($T_{\text{eff}}=5800$ K, representing solar case), G5V ($T_{\text{eff}}=5300$ K), and F7V ($T_{\text{eff}}=6300$ K). We note that the G5V and F7V classes encompass roughly 50% of the presently known planetary hosts. We account for a range of metallicity values between -1 and 0.9 dex which covers most planetary hosts. We first consider the development of the Sun-Earth system in the past 0.5 billion years as a model for planets and their host stars, during which the atmosphere was oxygenated and complex life on land evolved. We then study the dependence of surface UV irradiation on the atmospheric O₂ content and stellar metallicity. We show that the development of complex life on planets in the habitable zone can be sustained from a few percent of O₂ upward, being robust for a large range of stellar characteristics and against major extraterrestrial cataclysms.

Results

Figure 1 presents stellar spectra calculated for different metallicity values using the recent MPS-ATLAS code¹⁷. The UV flux drops substantially with increasing metallicity, creating seemingly more favourable conditions for life¹⁸. However, Fig. 1b shows that metallicity affects radiation in the O₃-producing Herzberg continuum much more strongly than in the O₃-destroying Hartley band. Thus, the net photochemical effect leads to a decrease of O₃ with metallicity, making the assessment of the UV conditions and potential habitability at the planetary surface less straightforward, which was hitherto not accounted for.

We consider hypothetical Earth-twin planets (with an N₂/O₂ atmosphere, water and terrestrial mass) in the habitable zones of stars

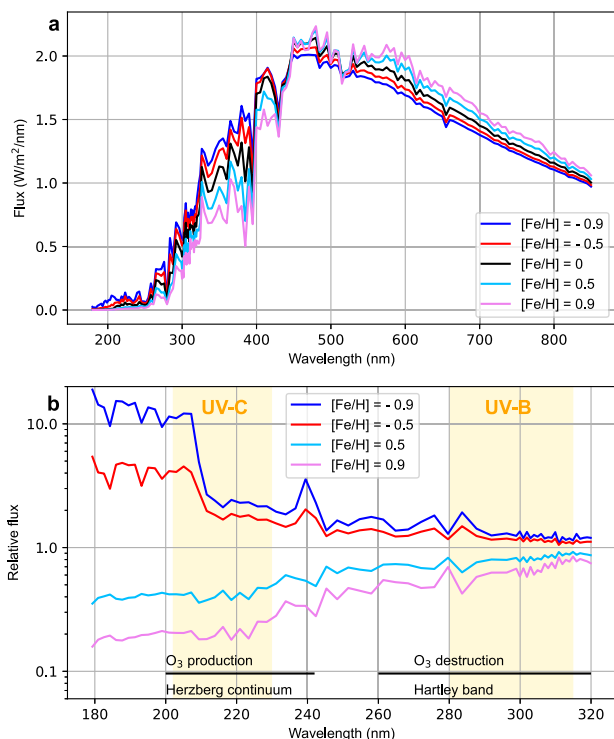


Fig. 1 | Stellar radiative spectra. **a** Stellar spectra calculated for different metallicities $[\text{Fe}/\text{H}]$ and a solar effective temperature T_{eff} of 5800 K. The calculations were performed for a spectral range of 170 to 850 nm and the total flux normalized to the solar constant. **b** The same as **a** but the flux is shown relative to the solar flux ($[\text{Fe}/\text{H}] = 0$). Radiation in the 200 to 242 and 260 to 320 nm intervals participates in O₃ production and destruction, respectively. These spectral ranges are defined by black solid lines. The yellow shaded areas show the spectral ranges of the UV-C reaching the lower atmosphere (202 to 230 nm, left) and UV-B (280 to 315 nm, right). Source data are provided as a Source Data file.

with T_{eff} and $[\text{Fe}/\text{H}]$ in ranges introduced above. The O₃ concentration in planetary atmospheres and the associated surface UV levels were computed with a coupled photochemical radiative-convective model¹⁹. The model has been designed and updated for accurate calculations of atmospheric O₃ chemistry. It avoids assumptions of fixed boundary conditions, e.g. of methane (CH₄) concentrations, and interactively computes the oxidation capacity of the atmosphere for different UV conditions, which is relevant for the removal of hazardous and greenhouse gases. The radiative scheme has a high spectral resolution, which appears to be critical for studying the impact of stellar radiation on planetary atmospheres⁴. The description of the planetary atmospheric model and our calculations of the input stellar spectra are presented in the methods sections Atmospheric model and Stellar spectra. We consider three key factors for a life-supporting UV environment on surfaces of planets: (1) UV-C level (relevant in low oxygen atmospheres); (2) the oxidation capacity of the lower atmosphere (regulated by UV radiation); (3) UV-B level (e.g., regarding DNA damage^{2,3}). Further, the atmospheric protection mechanism should be able to tolerate large disturbances, e.g. by volcanic eruptions and supernova explosions (which can destroy O₃^{20,21}) as well as changes of the activity of the host star²² which affects its radiation spectrum²³ (see methods sections Ozone and UV-B response to perturbations and Stellar spectra).

The Sun-Earth evolution

A quantitative assessment of the biological impact of these factors is challenging because additional protection (e.g. water bodies, shadowing by rocks, pigment formation) and biological repair mechanisms are not known. Therefore we considered the Earth-Sun system as a paradigm to guide the interpretation of our results for other systems. We first investigated how life on land of our planet steered through the conditions mentioned above and then how these conditions are affected by the effective temperature and metallicity of the host star.

Figure 2 illustrates the development of the Earth's atmosphere and surface UV fluxes over the last 600 Myr (million years before present). The geological isotope records indicate that the level of atmospheric O₂ (and CO₂, see Supplementary Table 1) went through substantial fluctuations^{24–27} (Fig. 2a). The largest change in O₂, known as the Paleozoic oxygenation event, happened around 470 Myr²⁸ when Earth's atmosphere went from almost anoxic to oxygenated conditions. While this event is absent in the reconstruction of Berner et al.²⁴ (B6, blue curve in Fig. 2a) data (probably because of simplified assumptions about sulfur geochemistry²⁹), it is evident in the more recent reconstruction of Lenton et al., 2016²⁷ (L16, light blue curve in Fig. 2a).

Before the Paleozoic oxygenation O₂ was mainly produced by aquatic photosynthesis in UV tolerant cyanobacteria and algae^{26,30,31} which could only provide a limited amount of O₂: while L16 indicates 4% of O₂ shortly before the event, other studies point to lower values of 2%³² or even 0.2%^{26,33}. It is understood that the Paleozoic oxygenation event was caused by the advent of the earliest land plants^{27,29}. This transition likely represents an important bottleneck: effective O₂ release to the atmosphere is not possible without land plants, which in turn are susceptible to UV radiation^{33,34} and can only appear when the O₂ concentration is sufficiently high to create a protective ozone layer. We have modelled the history of the Earth's atmosphere to calculate the O₂ and O₃ concentrations needed to overcome the oxygenation bottleneck on Earth and simultaneously establish quantitative criteria on the non-hostile level of UV irradiance.

Here we consider the evolution of UV-C and UV-B fluxes at the surface. While UV-C is particularly harmful to living cells due to the highly energetic photons, Fig. 2b shows that a flux of 10^{-3} Wm⁻², corresponding to a tolerable annual dose in the order of 10^4 J m⁻²³⁵, is achieved already at 0.3% of O₂. This is below the O₂ level after the Paleozoic oxygenation event. It is also below or comparable to

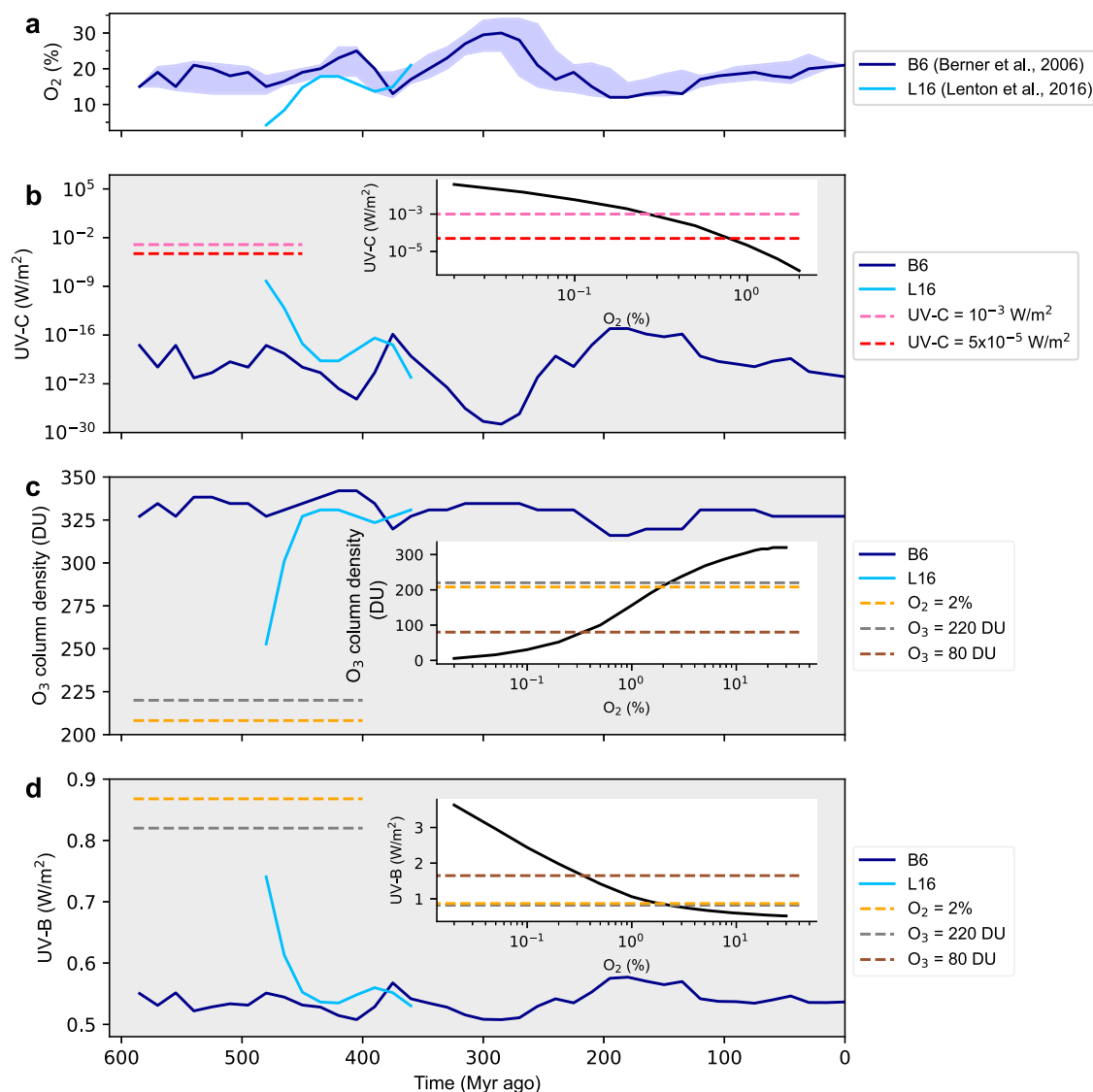


Fig. 2 | Evolution of atmospheric O_2 , O_3 column density and surface UV. a O_2 volume fraction of the Earth's atmosphere during the past 600 million years according to Berner et al., 2006²⁴ (B6, blue) and Lenton et al.²⁷ (L16, light blue). The blue shaded area indicates the uncertainty range of the B6 data. **b–d** Surface UV-C (202 to 230 nm) **b**, O_3 column density **c** and surface UV-B (280 to 315 nm) **d** ($1 \text{ DU} = 2.687 \times 10^{20} \text{ molecules/m}^2$). The blue and green curves are calculated with B6

and L16 data, respectively. The inserted plots show the dependencies of UV-C **b**, O_3 column density **c** and UV-B **d** on the O_2 content. **c**, **d** The level of O_3 corresponding to 2% of O_2 is shown by the yellow dashed line. The O_3 level of 220 and 80 DU are indicated by the grey and brown dashed lines, respectively. The UV-C levels of 10^{-3} and $5 \times 10^{-5} \text{ W/m}^2$ are shown by the pink and red dashed lines in **b**. Source data are provided as a Source Data file.

available estimates for the O_2 levels preceding the event^{27,32,33}. All in all, we do not expect the UV-C irradiance to pose a critical threat to the advent of land plants directly. Long CH_4 lifetimes resulting from our calculations, being a metric of the atmospheric oxidation capacity, indicate that the low UV-C values allow a mildly oxidative environment supporting the removal of hazardous gases in the lower atmosphere while not exposing organisms to harmful oxidant levels. It means that the atmosphere is not chemically aggressive, i.e. hostile to the organic molecules of living cells at $UV-C < 5 \times 10^{-5} \text{ W/m}^2$ or $O_2 > 0.8\%$ (Figs. 2b and 3e and Supplementary Fig. 5k). Under these more moderately oxidative conditions, the CH_4 lifetime exceeds about a year and thus does not drop below about a tenth of that in the atmosphere of today.

Since UV-B is mainly absorbed by O_3 , the surface UV-B level must be calculated together with the atmospheric chemistry and O_3 concentration. We show the results of such calculations in Fig. 2c, d. Previous work² has shown that O_3 column density is resilient even to strong changes of O_2 (Fig. 2c). Our study reveals that the Paleozoic oxygenation event, which corresponds to a change in O_2 by a factor of

4.5 (L16 data), resulted in a mere 30% change of O_3 column density (from 252 to 330 Dobson Units, DU) leading to a moderate UV-B response (from 0.75 to 0.55 W/m^2 , Fig. 2d). The low sensitivity of O_3 column density and, consequently of UV-B, to changes in O_2 is explained by the vertical adjustment of the ozone layer. Smaller O_2 amounts cause the ozone layer to form in lower and denser atmospheric layers where more O_2 is available for O_3 production (Supplementary Fig. 3a, b), leaving the total O_3 column density only weakly affected³⁶.

The total O_3 column density of 252 DU (Fig. 2c) calculated for the conditions shortly before the Paleozoic oxygenation event is well above the 220 DU (grey dashed line in Fig. 2c) that define the recent ozone hole over Antarctica²¹ and can be considered tolerable by the vegetation. Since the O_2 concentration before the Paleozoic oxygenation event is rather uncertain we consider even lower oxygen levels. Lowering O_2 to 2% results in O_3 decrease to 205 DU (orange dashed line in Fig. 2c) and a UV-B increase to 0.87 W/m^2 (Fig. 2d). Though this amount of O_3 qualifies as an ozone hole, it is routinely

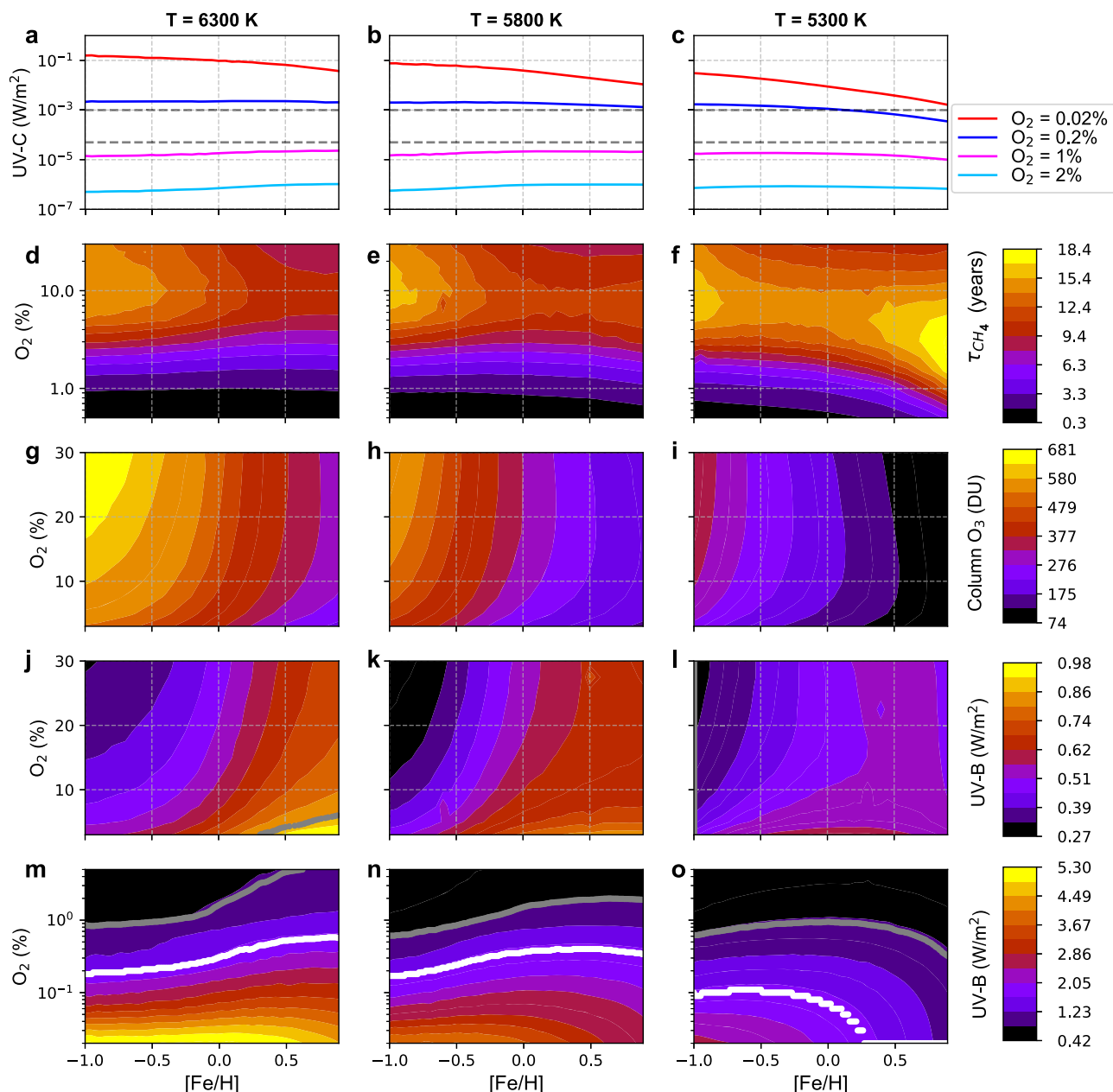


Fig. 3 | Metallicity impacts on the atmosphere. **a–c** The change of surface UV-C (202 to 230 nm, W/m^2) with $[\text{Fe}/\text{H}]$ for O_2 levels of 2% (light blue), 1% (magenta), 0.2% (blue) and 0.02% (red). The dashed lines indicate the UV-C levels of 5×10^{-3} and $10^{-3} \text{ W}/\text{m}^2$. **d–f** Impact of O_2 content and $[\text{Fe}/\text{H}]$ on CH_4 lifetime. **g–i** Dependencies of O_3 column density (**g–i** DU) and surface UV-B (**j–l** W/m^2) on O_2 content and stellar

metallicity $[\text{Fe}/\text{H}]$. **m–o** The same as **j–l** but for an O_2 content less than 5%. **a–o** The calculations were performed for stellar T_{eff} of 6300 K (left), 5800 K (center) and 5300 K (right). The grey and white curves (**j–o**) represent surface UV-B of 0.82 W/m^2 (220 DU, ozone hole definition) and 1.65 W/m^2 (80 DU, extreme in ozone hole), respectively. Source data are provided as a Source Data file.

measured over the Antarctic coastline³⁷ and sometimes over southern Argentina³⁸ or northern Europe where land plants are nevertheless abundant. Thus, also this level of UV-B does not pose a lethal threat to the terrestrial biosphere. The O_3 column density and UV-B modelled for O_2 below 2% are presented in the inserts of Fig. 2c, d. The O_3 column density of 80 DU (brown dashed line in Fig. 2c) that corresponds to O_2 of 0.3% is close to the lowest value measured over Antarctica in spring (September 30, 1994, with 73 DU) which was tolerable only due to the large solar zenith angle near the pole and the limited time period. Here, we consider the corresponding UV-B level of 1.65 W/m^2 (Fig. 2d) as the highest value that is known to be survivable by land plants on present Earth.

Our calculations thus show that the dependence of the surface UV-B fluxes on the O_2 amount is limited. We consider this to be a key

factor, together with the atmospheric oxidation capacity, for allowing land plants on Earth, which might similarly apply to habitable planets orbiting other stars. Furthermore, during the past 470 million years the dependence of the Earth's surface UV-B fluxes on the O_2 amount has been limited because the O_2 mixing ratio was well above 1%. Together with the atmospheric oxidation capacity, we consider this crucial for land plants on Earth, which might similarly apply to habitable exoplanets.

Impacts of stellar properties

The UV emission by a star strongly depends on fundamental stellar parameters. It increases with the stellar effective temperature T_{eff} ^{5–7} (Supplementary Fig. 2) and decreases with the metallicity $[\text{Fe}/\text{H}]$ (Fig. 1). We investigated how these parameters affect the

correspondence between O_2 in the planetary atmosphere and the surface UV thresholds indicated above. Note that O_2 in exoplanetary atmospheres may also be provided by abiotic sources^{39,40}. Figure 3a–c shows that for 1% of O_2 the surface UV-C flux is lower than the level of $5 \times 10^{-5} \text{ W/m}^2$ for all stellar T_{eff} and $[\text{Fe}/\text{H}]$ values. We find that for 0.2% or more O_2 the higher UV-C fluxes of metal-poor stars are compensated by higher O_3 concentrations resulting in almost metallicity-independent UV-C at the planetary surface (Fig. 3a–c and Supplementary Fig. 4). This is remarkable given the strong anti-correlation of stellar UV-C emission fluxes and metallicity (Fig. 1b). Interestingly, the UV-C level also marginally depends on stellar T_{eff} . Thus, the O_2 level that provides UV-C protection is very similar for a large range of stellar parameters.

In the case of very low O_2 (< 0.7%), UV-C photolysis of H_2O controls the formation of oxidants like excited O atoms and hydroxyl (OH) radicals (the latter known as the detergent of the atmosphere), which act as sinks for CH_4 and other molecules released from geochemical processes. Consequently the lifetime of CH_4 (τ_{CH_4}), which signifies the oxidation capacity of the atmosphere (Fig. 3d–f), is very short (below 1 year), which likely makes the planetary environment harmful for life on land. For O_2 in excess of about 0.7% the OH concentration (Supplementary Fig. 5j–l) and τ_{CH_4} are controlled by UV-B photolysis of O_3 , modulated by ambient concentrations of H_2O , NO_x (mostly NO, NO_2) and CO. While surface O_3 for O_2 levels between 0.7 and 2% strongly depends on T_{eff} and metallicity (Supplementary Fig. 5d–f), UV-B in the lower planetary atmosphere responds much less sensitively (Fig. 3m–o), and so does τ_{CH_4} (Fig. 3d–f). Above 2–3% O_2 , the atmospheric oxidation capacity is buffered, hence stable and benign to life, maintaining a τ_{CH_4} within 8–18 years throughout the range of $[\text{Fe}/\text{H}]$ and T_{eff} . For details about the temperature and atmospheric composition, see methods section Atmospheric model and Supplementary Fig. 5.

The effects of the stellar temperature T_{eff} and metallicity $[\text{Fe}/\text{H}]$ on UV are stronger in the Herzberg continuum, driving the chemical O_3 production, than in the Hartley band which drives O_3 destruction (see Fig. 1 for the $[\text{Fe}/\text{H}]$ effect and Supplementary Fig. 2 for the T_{eff} effect). As a result, the net photochemical effect leads to the increase of the O_3 column density with T_{eff} and a decrease with $[\text{Fe}/\text{H}]$ (Fig. 3g–i). Thus, changes in UV irradiance at the planetary surface can respond in the opposite direction to those of the stellar UV radiance. The net photochemical effect is not sufficiently strong to reverse the UV-B surface flux dependence on T_{eff} for all metallicities and oxygen levels (Fig. 3j–l, Supplementary Fig. 2), but it generally reverses the dependence on $[\text{Fe}/\text{H}]$ leading to the paradoxical anti-correlation of the surface and space UV-B fluxes (Figs. 1 and 3j–l). The increase of the surface UV-B with $[\text{Fe}/\text{H}]$ is especially strong for T_{eff} values of 5800 and 6300 K but it is less pronounced for 5300 K stars (where surface UV-B starts to decrease with $[\text{Fe}/\text{H}]$ for low O_2 levels, see Fig. 3o).

The white lines in Fig. 3m, n indicate that for the T_{eff} values of 5800 and 6300 K approximately two times more O_2 is needed to attain the extreme ozone hole conditions (i.e. UV-B flux of 1.65 W/m^2) for $[\text{Fe}/\text{H}] = 0.9$ than for $[\text{Fe}/\text{H}] = -1$. The oxygen concentration required to arrive at lower UV-B levels such as ozone hole conditions (0.82 W/m^2 , black lines in Fig. 3k–o) depends even more strongly on the metallicity for 5800 K and 6300 K stars. For example, for the effective temperature of the Sun the required O_2 concentration increases from 0.6% at $[\text{Fe}/\text{H}] = -1$ to about 2% for $[\text{Fe}/\text{H}] > 0.5$. The 5300 K stars do not show such a dependence. For example, the O_2 value needed for the UV-B flux of 0.82 W/m^2 marginally increases from an $[\text{Fe}/\text{H}]$ of -1 to ≈ 0 but decreases for higher $[\text{Fe}/\text{H}]$ (see black line in Fig. 3o).

Interestingly, the surface UV-B fluxes corresponding to atmospheres with an O_2 level higher than 3% monotonically increase with $[\text{Fe}/\text{H}]$ for all three T_{eff} values considered in this study (Fig. 3j, k, l, with the exception of $[\text{Fe}/\text{H}] \geq 0.8$ and $T_{\text{eff}} = 5300 \text{ K}$, see Fig. 3l). For example, for the T_{eff} of the Sun the increase of $[\text{Fe}/\text{H}]$ from -1 to 0.9 doubles

the surface UV-B flux. While surface UV-B fluxes on planets with oxygenated atmospheres may not pose a fatal threat for life on land, their increase with $[\text{Fe}/\text{H}]$ could negatively affect the evolution of life, especially for planets with low O_2 atmospheres, orbiting 5800–6300 K, high-metallicity stars. Since supernovae continuously enrich the Universe with heavy elements over time, stars that form later increasingly contain heavy elements and their planets provide less favourable UV conditions for vegetation and the advancement of complex land life.

While a high stellar metallicity causes UV-B stress for developed life in oxygenated atmospheres, it might be accompanied with faint UV-C radiation levels, being insufficient for the photochemical formation of essential macromolecular building blocks of life in early anoxic atmospheres. For example, it was recently estimated¹⁰ that the average UV actinic flux between 200 and 280 nm should exceed about $6 \times 10^9 \text{ cm}^{-2} \text{ s}^{-1} \text{ \AA}^{-1}$ at the planetary surface to allow abiogenesis. Supplementary Figs. 6 and 7 show the dependence of the surface actinic flux on the effective temperature T_{eff} and metallicity $[\text{Fe}/\text{H}]$ for the 80%-nitrogen and 20%-carbon dioxide atmosphere calculated using the atmospheric transmission dependence on wavelength adopted from Rimmer et al.¹⁰ (we note that in contrast to the oxygenated atmospheres the opacity in anoxic atmospheres is not affected by the net photochemical effect and, thus, is not expected to depend on the stellar spectrum). The actinic flux decreases for cooler and for metal-rich stars, making them less life-friendly. In particular, the actinic flux drops below the Rimmer et al.¹⁰ estimate for 5300 K metal-rich stars.

Discussion

A key factor for the development of land life is the stability of the atmospheric UV shielding in response to major disturbances that are likely to happen on geological time scales. We performed sensitivity simulations to study the atmospheric effects of potentially catastrophic events such as sudden increases of stellar activity, supernovae and volcanic eruptions. Our model results show that independent of the stellar metallicity such cataclysms do not pose planetary scale, existential threats to life (see methods section Ozone and UV-B response to perturbations and Supplementary Figs. 8–10). While the largest supervolcanoes on Earth have occasionally caused major species extinctions, there are no known examples of such events that have annihilated life⁴¹.

Our results show that from a few percent of O_2 upward and for a variety of stellar properties the surface UV exposure on Earth-like planets in habitable zones is likely to sustain the development of land plants that are essential for the further evolution of complex life. It includes a stable oxidation capacity of the atmosphere, which controls greenhouse gases such as CH_4 , contributing to favourable temperature conditions, while removing hazardous gases that would otherwise reach toxic levels. Paradoxically, whereas stars with higher metallicity, which have appeared later in the history of the Universe, emit less UV radiation, in oxygenated planetary atmospheres the associated stellar radiative spectrum allows less O_3 formation, which enhances UV penetration, making the conditions on planets orbiting these stars less friendly for the biosphere on land (except for 5300 K metal-rich stars and low O_2 atmospheres). The relatively low UV emission from the high-metallicity stars can also be a hurdle for the origin of first life on planets with anoxic atmospheres.

We thus find that the surface of planets orbiting metal-rich stars is exposed to more intense UV radiation than the surface of planets orbiting metal-poor stars. Therefore planets in the habitable zones of stars with low metallicity are the best targets to search for complex life on land. For the stellar types considered, metallicity has a larger impact on the surface UV than the stellar temperature. The atmospheric oxidation (cleaning) capacity is found to be stable and life-supporting, almost independent of stellar metallicity at an oxygen volume fraction above 1%.

The new generation of radial velocity (RV) spectrometers will be able to measure stellar reflex motion with a precision of 10 cm s^{-1} ⁴² which suffices to discover Earth-like planets in the habitable zones of Sun-like stars. Detecting Earth-like planets orbiting Sun-like stars is also the main objective of the upcoming PLANetary Transits and Oscillations (PLATO)⁴³ of stars space telescope. Our results indicate that to maximise the likelihood of finding signatures of life, planets hosted by low-metallicity stars discovered by these instruments should be priority targets of the follow-up observations with future telescopes⁴⁴.

The recently commissioned James Webb Space Telescope (JWST)⁴⁵ targets atmospheres of rocky planets around red dwarfs, i.e. stars significantly cooler and smaller than the Sun (since the signal from planets orbiting Sun-like stars is too low to be detected). While planets orbiting red dwarfs are not within the parameter range considered here, one future application of our model will be to simulate the spectral fingerprints of planetary atmospheres^{5,6,46–49} observable by JWST as well as anticipated ground-based facilities (like a 2040 s Large Infrared/Optical/Ultraviolet Space Telescope⁵⁰).

Methods

Atmospheric model

We applied an updated, global one-dimensional radiative-convective model of a primarily nitrogen/oxygen atmosphere with interactive chemistry¹⁹ for simulations of a wide range of O_2 levels and UV-spectra dependent on stellar properties and chemical perturbations. Photolysis rates are calculated with fine spectral resolution (176 wavelength intervals, delta-two-stream method) using equinox conditions and 6 zenith angles for the calculation of daytime average radiation fluxes, taking into account scattering and absorption interactively. Short-lived chemical species are assumed to be in local steady state, while longer-lived ones and chemical families are vertically redistributed by an eddy transport parameterisation. O_3 is part of the odd oxygen-family which also contains atomic oxygen in the ground and excited states and radicals of the rate limiting reactions in catalytic destruction cycles of the form



X can be NO, OH or halogen atoms. NO and OH are produced in the middle atmosphere from reaction of an excited O-atom from O_3 photolysis in the UV-B with N_2O and H_2O , respectively. Destruction of odd oxygen also occurs via the Chapman-reaction, which slows down with lower temperatures, e.g. due to radiative cooling by CO_2 :



O_3 production is governed by the photolysis of molecular oxygen by UV-radiation with wavelengths shorter than 242 nm, followed by



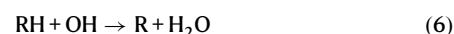
with M an arbitrary atmospheric molecule (e.g. N_2 , O_2).

The greenhouse gases H_2O , CO_2 , CH_4 , O_3 , and N_2O , predominant on Earth, are included in the near and terrestrial infrared radiative transfer calculations. Short-wave radiation reflected to space is determined from the high spectral resolution module used for the photolysis calculations. In the radiation calculations a climatological cloud cover is included and the surface albedo is fixed at conditions on Earth. The surface temperature (Supplementary Fig. 5) is calculated from the radiation budget at the top of the atmosphere, considering

the dependence of the near-infrared part of the stellar spectrum on the effective temperature of the star. It is assumed that the total incoming radiative energy flux at the top of the planetary atmosphere is the same as the solar constant for present day Earth. Lower atmospheric temperatures are calculated from an approximately moist adiabatic lapse rate while middle atmospheric temperatures result from radiative equilibrium. The water vapor feedback for greenhouse warming, i.e. through evaporation from the surface, is included by assuming a fixed relative humidity profile in the lower atmosphere.

The surface boundary conditions for O_2 and CO_2 on paleo-Earth are established following available geological reconstructions^{24,25,27}, see Supplementary Table 1. For the atmospheres of exoplanets CO_2 volume mixing ratios were fixed to preindustrial (Holocene) conditions on Earth.

Because of the paucity of geological data we used pre-industrial lower boundary conditions for CH_4 , N_2O , NO_x , and CO fluxes (230 Tg/yr, 12 Tg/yr, 30 Tg/yr NO_2 , 1500 Tg/yr, respectively, CO fluxes include oxidation products of volatile organic compounds from land plants) in all simulations. Typical results for the surface are shown in Supplementary Fig. 5. The oxidation of organic substances such as CH_4 proceeds via



where $\text{R} = \text{CH}_3$ in the case of methane. In the presence of NO_x the further oxidation of R leads to a recycling of OH. The NO_x originates from soil emissions (bacteria), lightning and N_2O breakdown in the middle atmosphere. Primary production of OH proceeds by reaction of an excited oxygen atom from the photolysis of O_3 with H_2O , and in the case of very low oxygen content by the UV-C photolysis of H_2O (Supplementary Fig. 5). The altitude of the maximum O_3 concentration, which decreases with stellar metallicity, shifts downward following the oxygen mixing ratio (Supplementary Fig. 3).

Ozone and UV-B response to perturbations

In Supplementary Fig. 8b–e we show the O_3 column density and surface UV-B levels calculated for the reference simulation, (black), conditions corresponding to a sudden increase of solar magnetic activity (yellow), a supernova explosion (magenta), and a major volcanic eruption (green), to test the stability of atmospheric conditions and compare with previous work. The reference simulation represents the pre-industrial Holocene state of the Earth's atmosphere (i.e. surface fluxes of CH_4 , N_2O , NO_x and CO are set to pre-industrial levels) under a stellar radiation intensity according to the minimum of solar cycle 22.

The high activity simulations are forced by the solar spectrum calculated for the Sun with an S-index value of 0.25, which corresponds to a magnetic activity level five times higher than during the maximum of solar cycle 22. This is motivated by the recent analysis of data from the Kepler space telescope³¹ and Gaia space observatory⁵² which hinted that the Sun might go through occasional epochs of high magnetic activity^{22,53}. The intensification of stellar activity results in an increase of UV emission (Supplementary Fig. 11) that is stronger for radiation with shorter wavelength²³. Consequently, the O_3 production rate increases more strongly than the destruction rate resulting in an increase of the total O_3 column density (Supplementary Fig. 8b). This result agrees with previous studies of the O_3 response to the solar activity cycle^{54,2} which also reported a positive correlation between O_3 column density and solar magnetic activity. The increase in O_3 enhances the protection from UV-B which overcompensates the increase of the solar UV-B for an O_2 content larger than 3% and damps it for smaller O_2 amounts. Consequently, the increase of stellar magnetic activity does not pose a serious threat to the biosphere in terms of UV-B exposure.

Another potential perturbation is a supernova explosion of a neighbouring star^{14,55} that increases the flux of charged particles

entering the planetary atmosphere²⁰. On Earth, most particles are deflected by the heliospheric and geo-magnetic fields, but a fraction enters the atmosphere and produces NO_x from molecular N₂ and O₂. While NO_x is capable of destroying O₃ in catalytic cycles in the upper and middle atmosphere, it can lead to O₃ production in the lower atmosphere^{14,21,55}. To simulate the response of the planetary atmosphere to supernovae we used a previous approach to estimate terrestrial O₃ depletion²⁰. We increased the NO production by charged particles by a factor of 100 relative to the reference simulation (which roughly corresponds to the effect of supernova exposure at 10 pc). The resulting O₃ column density and surface UV-B are shown in Supplementary Fig. 8 by the magenta curves. We find that the supernovae impact on O₃ column density and surface UV-B is weak, in agreement with previous work (independent of metallicity and O₂ level). In oxygenated atmospheres (O₂ level more than ~2%) supernovae lead to O₃ destruction and an increase of surface UV-B. When the O₂ content is relatively low, the additional production of O₃ at lower altitudes in the atmosphere helps decrease the UV-B penetration (Supplementary Figs. 9 and 10 for T_{eff} of 5300 K and 6300 K, respectively).

Major volcanic eruptions can potentially damage the ozone layer^{13,56}. The release of sulfur dioxide leads to the formation of sulfate particles which facilitate heterogeneous reactions that activate halogen-containing radicals that cause O₃ destruction^{57,58}. Furthermore, volcanic eruptions can directly inject halogens into the ozone layer^{58,59}. To estimate potential volcanic impacts we increased the amount of sulfate particles by an order of magnitude. Reactive chlorine and bromine components were increased by injecting 3Tg HCl and 30Gg HBr per year into the lower stratosphere. This scenario mimics the end-Permian eruption of the Siberian Traps⁴¹. The resulting O₃ column density and surface UV-B changes are shown in Supplementary Fig. 8 by the green curves. The O₃-depleting effect of volcanism can be strong but weakens when the O₂ content reaches about 10%. The volcanic impact is slightly weaker for metal-poor stars but does not drop with O₂ content (see Supplementary Figs. 9 and 10 for T_{eff} of 5300 and 6300 K, respectively).

Stellar spectra

The stellar spectra for different T_{eff} and metallicity values [Fe/H] have been calculated with the MPS-ATLAS code¹⁷. The metallicity is defined relative to the solar metallicity:

$$[\text{Fe}/\text{H}] = \log(N_{\text{Fe}}/N_{\text{H}})_{\text{star}} - \log(N_{\text{Fe}}/N_{\text{H}})_{\odot} \quad (7)$$

where N_{Fe} and N_H are the numbers of Fe and H atoms per volume unit. The chemical composition was taken from Asplund et al.⁶⁰

For each set of T_{eff} and [Fe/H] values we first computed the stellar model atmosphere using the dependence⁶¹ of mixing-length parameters on T_{eff} and [Fe/H] normalised to return a solar value of 1.25⁶² for solar T_{eff} and [Fe/H]. We have accounted for the line blanketing using the Opacity Distribution Functions which were computed utilising more than 100 millions of atomic and molecular lines whose spectral shape was calculated for a turbulent velocity value of 2 km s⁻¹^{17,62}. We have also accounted for the missing UV opacity following the approach by Shapiro et al.⁶³.

The emergent stellar spectrum was calculated on 176 wavelength intervals exactly corresponding to our radiation code in the planetary atmospheric model (see section Atmospheric model) for 24 disk positions and then integrated over the full stellar disk. We have considered the same sources of opacity as for computing the stellar atmospheric models. In particular, a large number of spectral lines is needed for realistic calculations of the line haze which dominates the UV opacity.

Finally, the spectra have been scaled to preserve the amount of total radiative energy the planet receives. The spectra of the active Sun have been calculated following the approach by Shapiro et al.²³ as a function of the S-index which is a standard measure of stellar activity

and is proportional to the ratio of the fluxes in Ca II H and K lines and the nearby continuum⁶⁴.

Data availability

The data that support the findings of this study are available from the corresponding author upon request. Stellar normalized photon fluxes in the 176 spectral intervals for all metallicities and the three effective temperatures are available in source data file input_flux_photons_{T}.txt. Source data are provided with this paper. The data sets generated during the current study are available in the Edmond repository, <https://doi.org/10.17617/3.WGVDYV>. Source data are provided with this paper.

Code availability

The atmospheric and MPS-ATLAS codes used in the current study are available from the corresponding author on reasonable request.

References

1. Brasseur, G. & Solomon, S. *Aeronomy of the Middle Atmosphere: Chemistry and Physics of the Stratosphere and Mesosphere*. Reidel, Dordrecht (2005).
2. National Research Council. *Causes and effects of stratospheric ozone reduction: an update*. National Academy Press, Washington, D.C. <https://doi.org/10.17226/319> (1982).
3. Yu, S. & Lee, S. Ultraviolet radiation: DNA damage, repair, and human disorders. *Mol. Cell. Toxicol.* **13**, 21–28 (2017).
4. Catling, D. et al. Why O₂ is required by complex life on habitable planets and the concept of planetary “Oxygenation Time”. *Astrobiology*. **5**, 415–38 (2005).
5. Segura, A. et al. Ozone concentrations and ultraviolet fluxes on earth-like planets around other stars. *Astrobiology* **3**, 689–708 (2003).
6. Segura, A. et al. Biosignatures from earth-like planets around M dwarfs. *Astrobiology* **5**, 706–725 (2005).
7. Rugheimer, S., Segura, A., Kaltenecker, L. & Sasselov, D. UV surface environment of Earth-like planets orbiting FGKM stars through geological evolution. *Astrophys. J.* **806**, 137 (2015).
8. Buccino, A. P., Guillermo, A. L., & Mauas P. J. D. UV habitable zones around M stars, *Icarus*, 582, <https://doi.org/10.1016/j.icarus.2007.08.012> (2007).
9. Ranjan, S., Wordsworth, R. & Sasselov, D. D. The surface UV environment on planets orbiting M dwarfs: implications for prebiotic chemistry and the need for experimental follow-up. *ApJ* **843**, 110 (2017).
10. Rimmer, P. B. et al. The origin of RNA precursors on exoplanets. *Sci. Adv.* **4**, eaar3302 (2018).
11. Segura, A. Star-planet interactions and habitability: radiative effects. In: Deeg, H., Belmonte, J. (eds) *Handbook of Exoplanets*. Springer, Cham (2018).
12. McKenzie, R., Smale, D. & Kotkamp, M. Relationship between UVB and erythemally weighted radiation. *Photochem. Photobiol. Sci.* **3**, 252–6 (2004).
13. Benca, J. P., Duijnste, I. A. P. & Looy, C. V. UV-B-induced forest sterility: implications of ozone shield failure in earth’s largest extinction. *Sci. Adv.* **4**, e1700618 (2018).
14. Fields, B. D. et al. Supernova triggers for end-Devonian extinctions. *Proc. Natl Acad. Sci. USA* **117**, 21008–21010 (2020).
15. Kostogryz, N. M. et al. Stellar limb darkening - A new MPS-ATLAS library for Kepler, TESS, CHEOPS, and PLATO passbands. *Astron. Astrophys.*, **666**, id.A60, 18 pp <https://doi.org/10.1051/0004-6361/202243722> (2022)
16. Talmi, O. & Shaviv, G. The Influence of UV radiation on exoplanets’ habitability. *J. Aeronaut. Aerosp. Eng.* **28**, 47–68 (2013).
17. Witzke, V. et al. MPS-ATLAS: a fast all-in-one code for synthesising stellar spectra. *Astron. Astrophys.* **653**, 22 (2021). A65.

18. Schneider, A. C. & Shkolnik, E. L. HAZMAT. III. The UV evolution of mid- to late-m stars with GALEX. *Astron. J.* **155**, 122 (2018).
19. Brühl, C. & Crutzen, P. J. Scenarios of possible changes in atmospheric temperatures and ozone concentrations due to man's activities, estimated with a one-dimensional coupled photo-chemical climate model. *Clim. Dyn.* **2**, 173–203 (1988).
20. Crutzen, P. J. & Brühl, C. Mass extinctions and supernova explosions. *Proc. Natl Acad. Sci. USA* **93**, 1582–1584 (1996).
21. WMO (World Meteorological Organization), *Scientific Assessment of Ozone Depletion: 2018*, Global Ozone Research and Monitoring Project—Report No. 58, 588 pp., Geneva, Switzerland, <http://ozone.unep.org/science/assessment/sap> (2018).
22. Reinhold, T. et al. The Sun is less active than other solar-like stars. *Science* **368**, 518–521 (2020).
23. Shapiro, A. V., Shapiro, A. I., Gizon, L., Krivova, N. A. & Solanki, S. K. Solar-cycle irradiance variations over the last four billion years. *Astron. Astrophys.* **636**, A83 (2020).
24. Berner, R. A. GEOCARBSULF: a combined model for phanerozoic atmospheric O₂ and CO₂. *Geochim. Cosmochim. Acta* **70**, 5653–5664 (2006).
25. Royer, D. L., Donnadiou, Y., Park, J., Kowalczyk, J. & Godderis, Y. Error analysis of CO₂ and O₂ estimates from the long-term geochemical model geocarbsulf. *Am. J. Sci.* **314**, 1259–1283 (2014).
26. Lyons, T. W., Reinhard, C. T. & Planavsky, N. J. The rise of oxygen in earth's early ocean and atmosphere. *Nature* **506**, 307–315 (2014).
27. Lenton, T. M. et al. Earliest land plants created modern levels of atmospheric oxygen. *Proc. Natl Acad. Sci. USA* **113**, 9704–9709 (2016).
28. Brand, U. et al. Atmospheric oxygen of the paleozoic. *Earth-Science Rev.* **216**, 103560 (2021).
29. Krause, A. et al. Stepwise oxygenation of the paleozoic atmosphere. *Nat. Commun.* **9**, 408 (2018).
30. Kasting, J. F. & Siefert, J. L. Life and the evolution of Earth's atmosphere. *Science* **296**, 1066–1068 (2002).
31. Ehling-Schulz, M. & Scherer, S. UV protection in cyanobacteria. *Eur. J. Phycol.* **34**, 329–338 (1999).
32. Johnston, D. T., Wolfe-Simon, F., Pearson, A. & Knoll, A. H. Anoxygenic photosynthesis modulated proterozoic oxygen and sustained earth's middle age. *Proc. Natl Acad. Sci. USA* **106**, 16925–16929 (2009).
33. Liu, X.-M. et al. A persistently low level of atmospheric oxygen in earth's middle age. *Nat. Comm.* **12**, 351 (2021).
34. Rozema, J. et al. The role of UV-B radiation in aquatic and terrestrial ecosystems—an experimental and functional analysis of the evolution of UV-absorbing compounds. *J. Photochem. Photobiol. B: Biol.* **66**, 2–12 (2002).
35. Otake, M., Yoshiyama, K. O., Yamaguchi, H. & Hidema, J. 222 nm ultraviolet radiation C causes more severe damage to guard cells and epidermal cells of Arabidopsis plants than does 254 nm ultraviolet radiation. *Photochem. Photobiol. Sci.* **20**, 1675–1683 (2021).
36. Kozakis, T., Mendonca, J. M. & Buchhave, L. A. Is ozone a reliable proxy for molecular oxygen? I. The O₂-O₃ relationship for Earth-like atmospheres. *Astron. Astrophys.* **665**, 156 (2022).
37. Newman, P. A., Kawa, S. R. & Nash, E. R. On the size of the Antarctic ozone hole. *Geophys. Res. Lett.* **31**, L21104 (2004).
38. de Laat, A. T. J. et al. Extreme sunbathing: three weeks of small total O₃ columns and high UV radiation over the southern tip of South America during the 2009 Antarctic O₃ hole season. *Geophys. Res. Lett.* **37**, L14805 (2010).
39. Meadows, V. S. Reflections on O₂ as a biosignature in exoplanetary atmospheres. *Astrobiology* **17**, 1022–1052 (2017).
40. Meadows, V. S. et al. Exoplanet biosignatures: understanding oxygen as a biosignature in the context of its environment. *Astrobiology* **18**, 630 (2018).
41. Beerling, D., Harfoot, M., Lomax, B. & Pyle, J. The stability of the stratospheric ozone layer during the end-Permian eruption of the Siberian Traps. *Philos. Trans. R. Soc. A.* **365**, 1843–1866 (2007).
42. Crass, J., et al. arXiv:2107.14291 (2021).
43. Rauer, H. et al. The PLATO 2.0 mission. *Exp. Astron.* **38**, 249–330 (2014).
44. Seager, S. *Proc. Natl Acad. Sci. USA* **111**, 12634 (2014).
45. Gardner, J. P. et al. The James Webb space telescope. *Space Sci. Rev.* **123**, 485–606 (2006).
46. Juanola-Parramon, R. et al. Modeling and performance analysis of the LUVVOIR coronagraph instrument. *J. Astronom. Telescopes, Instrum. Syst.* **8**, id. 034001 <https://doi.org/10.1117/1.JATIS.8.3.034001> (2022).
47. Rugheimer, S., Kaltenecker, L., Zsom, A., Segura, A. & Sasselov, D. Spectral fingerprints of earth-like planets around FGK stars. *Astrobiology* **13**, 251–269 (2013).
48. Rugheimer, S. et al. Effect of UV radiation on the spectral fingerprints of Earth-like planets orbiting M stars. *The Astrophys. J.* **809**, 57 (2015b).
49. Rugheimer, S. & Katlenegger, L. Spectra of earth-like planets through geological evolution around FGKM stars. *Astrophys. J.* **854**, 19 (2018).
50. Harman, C. E. et al. Abiotic O₂ levels on planets around F, G, K, and M stars: possible false positives for life? *Astrophys. J.* **812**, 137 (2015).
51. Borucki, W. J. et al. Kepler Planet-Detection Mission: Introduction and First Results. *Science* **327**, 977 (2010).
52. Gaia Collaboration. The Gaia mission. *A&A* **595**, A1 (2016).
53. Işık, E., Shapiro, A. I., Solanki, S. K. & Krivova, N. A. Amplification of brightness variability by active-region nesting in solar-like stars. *Astrophys. J.* **901**, L12 (2020).
54. Shapiro, A. V. et al. The role of the solar irradiance variability in the evolution of the middle atmosphere during 2004–2009. *J. Geophys. Res. Atmospheres* **118**, 3781–3793 (2013).
55. Clery, D. Starstruck. *Science* **373**, 269–273 (2021).
56. Marshall, J. E. A., Lakin, J., Troth, I. & Wallace-Johnson, S. M. UV-B radiation was the Devonian-Carboniferous boundary terrestrial extinction kill mechanism. *Sci. Adv.* **6**, eaba0768 (2020).
57. Solomon, S. Stratospheric ozone depletion: a review of concepts and history. *Rev. Geophys.* **37**, 275–316 (1999).
58. Osipov, S. et al. The Toba supervolcano eruption caused severe tropical stratospheric ozone depletion. *Nat. Comm. Earth Environ.* **2**, 71 (2021).
59. Cadoux, A., Scaillet, B., Bekki, S., Oppenheimer, C. & Druitt, T. H. Stratospheric ozone destruction by the bronze-age minoan eruption (Santorini volcano, Greece). *Sci. Rep.* **5**, 12243 (2015).
60. Asplund, M., Grevesse, N., Sauval, A. J. & Scott, P. The chemical composition of the Sun. *Annu. Rev. Astron. Astrophys.* **47**, 481 (2009).
61. Viani, L. S. et al. Investigating the metallicity–mixing-length relation. *Astrophys. J.* **858**, 28 (2018).
62. Kurucz, R. L. Kurucz's WIDTH code and INPWIDTH. *Memorie della Societa Astronomica Italiana Supplementi* **8**, 86 (2005).
63. Shapiro, A. I., Schmutz, W., Schoell, M., Haberleiter, M. & Rozanov, E. A new approach to the long-term reconstruction of the solar irradiance leads to large historical solar forcing. *Astron. Astrophys.* **517**, A48 (2010).
64. Wilson, O. C. Chromospheric variations in main-sequence stars. *Astrophys. J.* **226**, 379 (1978).

Acknowledgements

A.V.S. and L.G. acknowledge funding from the Max Planck Society (grant “Preparations for PLATO science”). N.K. and L.G. acknowledge funding from the German Aerospace Center (DLR FKZ 50OP1902 “PLATO Data Center”). A.I.S. and V.W. were funded by the European Research Council

(ERC) under the European Union's Horizon 2020 research and innovation program (Grant no. 715947).

Author contributions

A.V.S. conducted the simulations and coordinated the writing of the manuscript. C.B. provided and adapted the model used for calculating the planetary atmosphere. C.B., K.K., B.S., and J.L. provided expertise on atmospheric physics and chemistry. N.K., V.W., and A.I.S. calculated the stellar spectra. A.I.S., L.G., and S.K.S. provided the expertise on stellar physics. A.V.S., A.I.S., C.B., K.K., and B.S. prepared the first draft. All authors contributed to the final manuscript. All authors discussed the results and reviewed the manuscript.

Funding

Open Access funding enabled and organized by Projekt DEAL.

Competing interests

The authors declare no competing interests.

Additional information

Supplementary information The online version contains supplementary material available at <https://doi.org/10.1038/s41467-023-37195-4>.

Correspondence and requests for materials should be addressed to Anna V. Shapiro.

Peer review information *Nature Communications* thanks Antígona Segura, and the other, anonymous, reviewer for their contribution to the peer review of this work. Peer reviewer reports are available.

Reprints and permissions information is available at <http://www.nature.com/reprints>

Publisher's note Springer Nature remains neutral with regard to jurisdictional claims in published maps and institutional affiliations.

Open Access This article is licensed under a Creative Commons Attribution 4.0 International License, which permits use, sharing, adaptation, distribution and reproduction in any medium or format, as long as you give appropriate credit to the original author(s) and the source, provide a link to the Creative Commons license, and indicate if changes were made. The images or other third party material in this article are included in the article's Creative Commons license, unless indicated otherwise in a credit line to the material. If material is not included in the article's Creative Commons license and your intended use is not permitted by statutory regulation or exceeds the permitted use, you will need to obtain permission directly from the copyright holder. To view a copy of this license, visit <http://creativecommons.org/licenses/by/4.0/>.

© The Author(s) 2023